Endoplasmic reticulum membrane receptors of the GET pathway are conserved throughout eukaryotes

Lisa Yasmin Asseck[a,b], Dietmar Gerald Mehlhorn[a,b], Jhon Rivera Monroy[c,d], Martiniano Maria Ricardi[b], Holger Breuninger[a], Niklas Wallmeroth[a], Kenneth Wayne Berendzen[a], Minou Nowrousian[b], Shuping Xing[a], Blanche Schwappach[c], Martin Bayer[e], and Christopher Grefen[a,b,1]

[a]Developmental Genetics, Centre for Plant Molecular Biology, University of Tübingen, 72076 Tübingen, Germany; [b]Department of Molecular and Cellular Botany, Ruhr-University Bochum, 44780 Bochum, Germany; [c]Department of Molecular Biology, University Medical Center Göttingen, 37073 Göttingen, Germany; [d]High-Complexity Instrument Laboratory, Universidad de La Salle, 110231 Bogotá, Colombia; and [e]Department of Cell Biology, Max Planck Institute for Developmental Biology, 72076 Tübingen, Germany

Edited by Natasha V. Raikhel, Center for Plant Cell Biology, Riverside, CA, and approved November 14, 2020 (received for review August 20, 2020)

Type II tail-anchored (TA) membrane proteins are involved in diverse cellular processes, including protein translocation, vesicle trafficking, and apoptosis. They are characterized by a single C-terminal transmembrane domain that mediates posttranslational targeting and insertion into the endoplasmic reticulum (ER) via the Guided-Entry of TA proteins (GET) pathway. The GET system was originally described in mammals and yeast but was recently shown to be partially conserved in other eukaryotes, such as higher plants. A newly synthesized TA protein is shielded from the cytosol by a pretargeting complex and an ATPase that delivers the protein to the ER, where membrane receptors (Get1/WRB and Get2/CAML) facilitate insertion. In the model plant *Arabidopsis thaliana*, most components of the pathway were identified through *in silico* sequence comparison, however, a functional homolog of the coreceptor Get2/CAML remained elusive. We performed immunoprecipitation-mass spectrometry analysis to detect in vivo interactors of *At*GET1 and identified a membrane protein of unknown function with low sequence homology but high structural homology to both yeast Get2 and mammalian CAML. The protein localizes to the ER membrane, coexpresses with *At*GET1, and binds to *Arabidopsis* GET pathway components. While loss-of-function lines phenocopy the stunted root hair phenotype of other *Atget* lines, its heterologous expression together with the coreceptor *At*GET1 rescues growth defects of *Δget1get2* yeast. Ectopic expression of the cytosolic, positively charged N terminus is sufficient to block TA protein insertion in vitro. Our results collectively confirm that we have identified a plant-specific GET2 in *Arabidopsis*, and its sequence allows the analysis of cross-kingdom pathway conservation.

GET pathway | tail-anchored proteins | SNAREs | ER membrane | root hairs

Membrane proteins are ubiquitous in all domains of life. In eukaryotes, approximately one-third of all open reading frames are identified or predicted to integrate with at least one transmembrane domain (TMD) into the lipid bilayer (1). Most membrane proteins are recognized as such at the ribosome during translation and are immediately inserted into the ER membrane via a pathway known as cotranslational insertion. Recognition of these membrane proteins is based on an N-terminal signal sequence or the first TMD and its isochronal detection by the signal recognition particle (SRP) on emergence from the ribosome.

A number of membrane proteins are neither recognized by the SRP nor cotranslationally inserted, however. Among these are the tail-anchored (TA) proteins, which feature a single C-terminal TMD that inserts into the ER membrane in a type II orientation; that is, the N-terminal part of the protein faces the cytosol. Important members of this membrane protein family are *N*-ethylmaleimide–sensitive factor attachment protein receptors (SNAREs) that catalyze membrane fusion events in eukaryotes (2–4). However, the absence of an N-terminal signal sequence in TA proteins dictates their insertion to be posttranslational and requires chaperoning of the mature protein through the cytosol to the membrane. The Guided-Entry of TA proteins (GET) pathway was found to perform the steps necessary for the task of receiving the nascent TA proteins, chaperoning these to the membrane and insert via dedicated receptors (5).

A pretargeting complex comprising Sgt2, Get4, and Get5 (metazoa: SGTA, TRC35, UBL4A, and BAG6) receives the TA protein from the ribosome (6, 7) and hands it over to the homodimer ATPase Get3 (TRC40) (6–9). Transfer of the TA protein to Get3 requires the hydrolysis of ATP (10, 11). The terminal insertion step is initiated through interaction of the Get3-TA complex first with the ER membrane receptor Get2 (CAML), followed by release of ADP and subsequent disassembly of the complex facilitated by interaction with Get1 (WRB) (12, 13). A stretch of positively charged amino acids within the cytosolic N terminus of Get2/CAML is required for Get3/TRC40 binding (14, 15).

The ER receptors of the GET pathway form an intricate relationship (16). Knockout of WRB in cardiomyocytes results in reduced protein levels of CAML. Interestingly, this difference is caused posttranslationally, as mRNA levels are not altered (17). Rather, the lack of sufficient protein level of WRB within the membrane leads to incomplete integration of CAML and its subsequent proteasomal degradation (18).

Significance

The GET pathway is required for the insertion of tail-anchored (TA) membrane proteins in the endoplasmic reticulum (ER) of yeast and mammals. Some orthologous genes had also been identified in higher plants with the exception of one of the two ER membrane receptors required for membrane insertion. Get2/CAML is required for the pathway's cytosolic chaperone to dock and release its TA protein cargo. Here we report the identification of the elusive plant GET pathway receptor through an interaction screen in *Arabidopsis*. The candidate allows detection of further Get2/CAML orthologs in higher plants, revealing conservation and function of structural features across kingdoms. Additionally, our results demonstrate that these features, rather than sequence conservation, determine functionality of the candidate within the pathway.

Author contributions: S.X., B.S., and C.G. designed research; L.Y.A., D.G.M., J.R.M., M.M.R., N.W., S.X., M.B., and C.G. performed research; K.W.B., M.N., and M.B. contributed new reagents/analytic tools; L.Y.A., H.B., K.W.B., M.N., B.S., M.B., and C.G. analyzed data; and L.Y.A. and C.G. wrote the paper.

The authors declare no competing interest.

This article is a PNAS Direct Submission.

[1]To whom correspondence may be addressed. Email: christopher.grefen@rub.de.

This article contains supporting information online at https://www.pnas.org/lookup/suppl/doi:10.1073/pnas.2017636118/-/DCSupplemental.

Published December 28, 2020.

While the GET pathway was originally described in opisthokonts (19, 20), it was recently shown to be partially conserved in other eukaryotes, such as Archaeplastida (21, 22). The main GET pathway components were identified through in silico analysis of protein sequence conservation (21, 22). In this way, orthologs for Get1/WRB, Get3/TRC40, Get4/TRC35, Get5, and Sgt2 were identified in *Arabidopsis thaliana*. Similar to the initial mystery around the existence of a functional Get2 ortholog in animals (15), our sequence analysis alone did not reveal potential candidates in higher plants.

Here we now report the identification and functional characterization of an archaeplastidic ortholog of the opisthokont Get2/CAML through an immunoprecipitation-mass spectrometry (IP-MS) approach. Using *At*GET1-GFP–expressing *Arabidopsis* plants, we detected an unknown membrane protein, At4g32680, which we temporarily assigned as G1IP (*At*GET1-interacting protein). The protein shows low sequence similarity to the opisthokont Get2/CAML but apparent conservation of structural features: a positively charged, cytosolic N terminus followed by three TMDs. T-DNA insertion and CRISPR loss-of-function lines phenocopy other *Atget* lines, while double-receptor knockouts do not show exacerbated effects, suggesting pathway conservation. G1IP together with *At*GET1 can complement the growth defects of the yeast receptor knockout, and expression of the charged stretch at the N terminus is sufficient to interrupt TA protein import in dog reticulocytes. Extensive interaction analyses revealed that G1IP interacts with other pathway components. Collectively, our results suggest that G1IP codes for a plant-specific GET2 that is functionally equivalent to its yeast and mammalian counterparts, although only TMDs and small sequence motifs are conserved across eukaryotes.

The protein sequence of *Arabidopsis* GET2 serves as an important puzzle piece in understanding cross-kingdom evolution of the GET pathway. It seems likely that the plant GET2 orthologs, fungi Get2, and mammalian CAML derived from a common ancestor, and that the evolutionary pressure was maintained on the structural features of a cytosolic, positively charged stretch at the N terminus and three TMDs at the C terminus.

Results and Discussion

An Unknown Transmembrane Protein Interacts with *At*GET1 and *At*GET3a In Planta. Both GET receptor-forming protein pairs Get1 and Get2 in yeast (19, 23), as well as WRB and CAML (15) in mammalian cells, have been shown to copurify. Thus, we chose affinity purification as a promising strategy to identify the elusive coreceptor of *At*GET1. We performed immunoprecipitation of *At*GET1-GFP stably expressed in *A. thaliana* wild-type (WT), Col-0, followed by mass spectrometry analysis. Two biological replicates were executed, and candidates that came up in both experiments and predicted to contain TMDs were considered high-confidence targets (Table 1).

Since both Get2 and CAML contain a C-terminal membrane-anchoring domain with three transmembrane helices, we focused on candidates with such a structure. We identified an unknown membrane protein, G1IP (*At*GET1-interacting protein; At4g32680), which appeared to match these preferences (Fig. 1*A*). Interestingly, G1IP was also detected in our previously published IP-MS results using *At*GET3a-GFP (22), substantiating that this protein may indeed be part of the *Arabidopsis* GET pathway. In addition, a close homolog of G1IP exists in *Arabidopsis* (At1g52343) that we termed G1IP-*like*. This protein was identified in both IP-MS analyses of *At*GET1, but not when using *At*GET3a-GFP as a target (22) (Table 1).

Multiple sequence alignment using MegaX showed only low overall similarity between G1IP and yeast Get2 or mammalian CAML, respectively (*SI Appendix*, Fig. S1*A*). However, structural comparison revealed that the predicted membrane topology of G1IP suggests a type II orientation with a long cytosolic N terminus, three transmembrane helices, and a luminal C-terminal region (TMHMM, Tmpred, and Protter version 1.0) (24) closely resembling the structure of yeast Get2 and mammalian CAML (Fig. 1*A*). Moreover, Phyre2 and HHpred analyses of the sequence maps part of the N terminus of G1IP (amino acids 6 to 27) with the crystal structure of cytosolic *Sc*Get2 bound to *Sc*Get3 (structures 3ZS9_D and 3SJD_E, respectively).

The predicted orientation of G1IP was experimentally verified using ratiometric bimolecular fluorescence complementation (rBiFC) (25) with the coreceptor *At*GET1 (*SI Appendix*, Fig. S1*B*). The putative structure of G1IP-*like* is similar to that of G1IP with a relatively large N-terminal cytosolic region and two or three transmembrane helices in the C-terminal domain, predicted via TMHMM or TMpred, respectively.

G1IP and *At*GET1 Share the Same Expression Profile and Subcellular Localization. To determine a functional relationship between G1IP and *At*GET1, we assessed the expression patterns by quantitative PCR (qPCR). Consistent with expression data of publicly available microarray and proteomics data (26), qPCR analysis revealed constitutive coexpression of G1IP and *At*GET1 at almost identical levels across all tissues and developmental stages, supporting the notion of a shared molecular pathway (Fig. 1*B*). In contrast, G1IP-*like* exhibited flower-specific gene expression in both qPCR and in silico analysis (eFP Browser), indicating functional divergence of the two homologs. Such an organ-specific expression pattern of G1IP-*like* most likely contradicts a putative housekeeping function that the *At*GET1 coreceptor needs to fulfill within the GET pathway. Instead, G1IP-*like* may have acquired novel, flower-specific functions independent of *At*GET1.

The *At*GET1 receptor was previously described as an ER-localized protein (22). However, in silico prediction suggests a nuclear localization for G1IP (suba.live/factsheet.html?id=AT4G32680.1), which would contradict a potential ER import function of a GET pathway coreceptor. To investigate the subcellular localization of G1IP in *A. thaliana*, we created stable transgenic plants that coexpress N-terminally GFP-tagged G1IP with the ER marker secRFP-HDEL. Using confocal laser scanning microscopy (CLSM), we were able to confirm a subcellular ER localization for G1IP (Fig. 1 *C*–*F*), as was demonstrated previously for *At*GET1 (22). Similar to its homolog, G1IP-*like* also localizes to the ER membrane (Fig. 1 *G*–*J*).

G1IP Binds *At*GET3a Only in the Presence of *At*GET1. To corroborate and expand the analyses of physical interaction of G1IP and G1IP-*like* with *Arabidopsis* GET pathway components, we performed rBiFC (25, 27, 28) and coimmunoprecipitation (co-IP) analyses. Complementation of the YFP signal, a cue for physical interaction, was detected only in samples in which *At*GET1 was coexpressed with G1IP or G1IP-*like* (Fig. 1 *K*–*M* and *SI Appendix*, Fig. S2 *A*–*C*). The residual YFP signal in samples with *At*GET3a was comparable to the biological negative control of *At*GET4, a protein found further upstream of the pathway that is unable to interact on its own with the receptors in yeast and mammals (7, 29). Given our identification of G1IP as a binding partner of *At*GET3a in our previously published IP-MS analyses (22), this lack of an interaction in rBiFC was somewhat surprising.

Therefore, we generated a new set of Gateway-compatible 2in1 co-IP vectors allowing for high constitutive gene coexpression in *Arabidopsis* (Fig. 1*N*). Interestingly, interaction was detected only in WT (Fig. 1*O*) and not in the *Atget1-2* mutant background (Fig. 1*P*), suggesting that the interaction of *At*GET3a and G1IP is highly sensitive to the presence or absence of *At*GET1 (see Fig. 4*C*). It was recently demonstrated that the human Get1 ortholog WRB is required for protein stability and correct insertion of CAML, the Get2 receptor in metazoa (18); however, we did not observe instability of ectopically expressed G1IP in *Atget1-2* mutants (Fig. 1*P*).

Table 1. AGI codes and identifiers of candidates identified in both replicates of *At*GET1-GFP IP-MS analyses and predicted to contain TMDs

			Prediction tool			
			Localization,	Number of TMDs		
AGI	Gene name	Description	SUBA	TMHMM	TMpred	Also detected via *At*GET3a-GFP (22)
AT4G32680	*G1IP*	Unknown transmembrane protein	Nuc	3	4 or 3	Yes
AT1G52343	*G1IP-like*	Unknown transmembrane protein	Cyt/Mito	2	3	No
AT5G13490	*AAC2*	ADP/ATP carrier 2	Mito	3	5 or 4	Yes
AT5G13430		Ubiquinol-cytochrome C reductase FeS subunit	Mito	0	2	Yes
AT1G50200	*ALATS*	Alanyl-tRNA synthetase	Mito	0	1	Yes
AT4G01100	*ADNT1*	Adenine nucleotide transporter 1	Mito	0	4	Yes
AT5G41670		6-phosphogluconate dehydrogenase family protein	Mito/Chp	0	2	Yes
AT2G38040	*CAC3*	Carboxyltransferase alpha subunit	Chp	0	3	Yes
AT1G64190		6-phosphogluconate dehydrogenase family protein	Chp	0	2	Yes
AT1G29900	*CARB*	Carbamoyl phosphate synthetase B	Chp	0	2 or 1	Yes
AT5G30510	*RPS1*	Ribosomal protein S1	Chp	0	1	No
AT5G53480		ARM repeat superfamily protein	Cyt/Nuc/Chp	0	3	No
AT2G20580	*RPN1A*	26S proteasome regulatory subunit S2 1A	Cyt/Nuc	0	5 or 4	Yes
AT4G24820		26S proteasome regulatory subunit Rpn7	Cyt/Nuc	0	1	Yes
AT2G30490	*C4H*	Cinnamate-4-hydroxylase	ER	0	2	Yes
AT5G47990	*CYP705A5*	Cytochrome P450 705A5	ER	0	4	Yes
AT1G07810	*ECA1*	ER-type Ca2 -ATPase 1	ER	8	9	Yes
AT3G51460	*RHD4*	Phosphoinositide phosphatase family protein	ER	2	3	Yes
AT1G70770		Protein of unknown function DUF2359	ER	0	2 or 1	Yes
AT4G21150	*HAP6*	Ribophorin II (RPN2) family protein	ER	4	4	Yes
AT1G29310		SecY protein transport family protein	Golgi	10	10 or 9	Yes
AT4G25820	*XTH14*	Xyloglucan endotransglucosylase/hydrolase 14	CW	1	1	Yes

Nuc, nucleus; Cyt, cytosol; Mito, mitochondria; Chp, chloroplast; CW, cell wall.

G1IP Phenocopies GET Pathway Mutants. We have previously shown that loss of some GET pathway components in *A. thaliana* leads to reduced root hair elongation under standard growth conditions (22). To investigate whether G1IP belongs to the same pathway, we analyzed the root hair growth of putative loss-of-function lines (Fig. 2*A* and *SI Appendix*, Fig. S3). The T-DNA insertion line *g1ip-3* showed significantly shorter root hairs at seedling level compared with WT Col-0 and similar to the *A. thaliana* GET pathway mutant *get1-1* (22) (Fig. 2*B*). Expression of a genomic version of the *G1IP* gene under the constitutively active VAMP721 promoter (*g1ip-3* compl.) restored WT-like root hair growth.

G1IP in Concert with *At*GET1 Can Complement Yeast GET Receptor Mutants. It had been demonstrated that the loss of GET pathway components in yeast results in a lack of (heat) stress tolerance (30). Therefore, we tested whether G1IP or G1IP-*like* are able to complement yeast growth under increasing temperatures (Fig. 2 *C* and *D*). The simultaneous expression of *At*GET1 and G1IP is able to weakly recover the viability of the *Δget1get2* strain (31), indicating at least some functional conservation between the *Arabidopsis* and yeast genes (Fig. 2*C*). However, coexpression of the *Arabidopsis* homolog G1IP-*like* together with *At*GET1 in *Δget1get2* is not able to rescue the lethality at higher temperatures, comparable to the vector-only control. The lack of a noticeable phenotype in *g1ip-like* lines, along with the different expression profile and lack of rescue of *Δget1get2* yeast, strongly suggest that G1IP-*like* has acquired a novel function independent of the GET pathway.

In another approach, we tested the importance of a heterologous or homologous partner receptor for yeast rescue (Fig. 2*D*). Mixing the corresponding receptors of the different species did not rescue as efficiently as the homologous combinations of *At*GET1/G1IP or *Sc*GET1/*Sc*GET2; however, the combination of *Sc*GET1 with G1IP appears to perform even weaker than the opposite combination with *At*GET1 and *Sc*GET2, mirroring an earlier observation with the mammalian GET2 ortholog CAML (30). This result implies that the eukaryotic Get2/CAML in general may have undergone more structural changes during evolution, making it more specialized as opposed to the more conserved GET1/WRB.

G1IP Interacts with the *At*GET1 Receptor via Its TMDs. Mammalian WRB and CAML have been previously shown to associate via interactions between their TMDs, thereby forming a functional receptor complex (15). Therefore, we examined the importance of the transmembrane region of G1IP in binding to *At*GET1 using rBiFC and co-IP. We separated the cytosolic tail (amino acids 1 to 173) of G1IP from its TMD region (amino acids 174 to 282) and tested both domains individually for *At*GET1 interaction (Fig. 3 *A* and *B* and *SI Appendix*, Fig. S2 *D* and *E*). Interaction of full-length G1IP with *At*GET1 in rBiFC resulted in strong YFP complementation, with a YFP:RFP ratio above the positive control *At*GET1 with *At*GET3a. While the ratio was lower using the truncated construct G1IP-TMDs, it nonetheless gave a strong signal of YFP complementation; however, the cytosolic part of G1IP showed an almost complete absence of signal comparable to the biological negative control of *At*GET1 and *At*GET4.

The rBiFC result was corroborated via co-IP by leveraging a 2in1 Förster resonance energy transfer (FRET) construct (35) transiently transformed in *Nicotiana benthamiana* (Fig. 3*C*). Fusion proteins of *At*GET1-EGFP coexpressed with mCherry-G1IP, mCherry-G1IPcyt, or mCherry-G1IP-TMDs were purified from tobacco leaf extracts via the RFP-trap antibody. After complex elution, immunoblotting against GFP revealed the presence of *At*GET1-GFP in eluates of G1IP and G1IP-TMDs but not of G1IPcyt (Fig. 3*D*). Our results indicate that G1IP acts as binding partner of *At*GET1 via its TMDs.

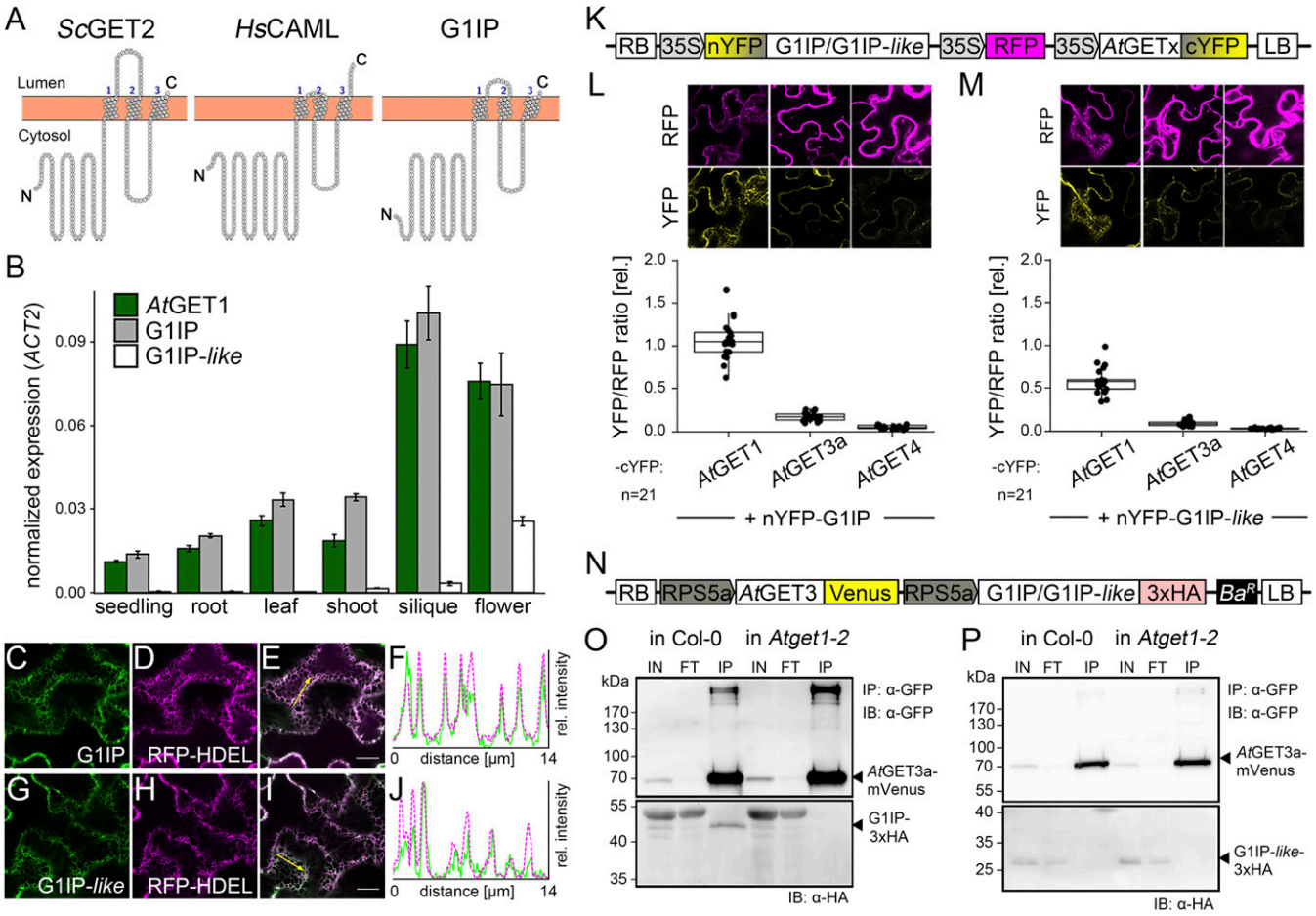

Fig. 1. G1IP coexpresses with *At*GET1, localizes to the ER, and interacts with *At*GET1 and *At*GET3a. (*A*) Transmembrane topology prediction of *Sc*GET2, *Hs*CAML, and G1IP using Protter. (*B*) Relative transcript levels of *At*GET1, G1IP, and G1IP-*like* in different organs of *A. thaliana* Col-0 plants measured by qPCR analysis. ACT2 was used as a reference gene. Error bars indicate SD. $n = 3$. (*C*–*J*) CLSM analysis of the subcellular localization of p35S::GFP-G1IP (*C*–*F*) and p35S::GFP-G1IP-*like* (*G*–*J*) in leaves of stably transformed *A. thaliana* lines coexpressing the ER marker RFP-HDEL. Line histograms (*F* and *J*) along yellow arrows in *E* and *I* confirm colocalization. (Scale bars: 10 μm.) (*K*) Schematic of the 2in1 rBiFC constructs used in *L* and *M*. (*L* and *M*) rBiFC analysis of G1IP (*L*) and G1IP-*like* (*M*) with *Arabidopsis* GET pathway components. Exemplary CLSM images of transiently transfected *N. benthamiana* leaves are depicted. Mean fluorescence levels of 21 areas were measured in YFP and RFP channels, ratioed, and plotted to show YFP complementation. The center lines of boxes represent the median with outer limits at the 25th and 75th percentiles. Tukey whiskers extend to 1.5 times the IQR. All values are depicted as black dots. (*N*) Schematic of the 2in1 co-IP constructs used in *O* and *P*. (*O* and *P*) Co-IP of *At*GET3a with G1IP (*O*) or G1IP-*like* (*P*) in Col-0 and *Atget1-2* mutant background. Protein extracts of *Arabidopsis* seedlings overexpressing *At*GET3a-mVenus and G1IP-3xHA or G1IP-*like*-3xHA were immunoprecipitated with anti-GFP beads. Protein–protein interaction was detected by immunoblotting using anti-GFP and anti-HA antibodies. IN, input; FT, flow-through; IP, immunoprecipitate.

Interference of the Cytosolic G1IP N Terminus in TA Protein Insertion. Despite the low level of sequence similarity between G1IP and yeast Get2 or mammalian CAML, multiple protein sequence alignment showed that a cluster of positively charged amino acids near the N terminus is conserved among the proteomes of vertebrates, plants, and fungal lineages (Fig. 3*E* and *SI Appendix*, Fig. S4). This motif is proposed to be crucial for binding of *Sc*Get3 (14) and its mammalian homolog TRC40 (15) and has been shown to segregate with the membrane-anchoring domain of Get2/CAML-*like* proteins in a position-specific iterative (PSI)-BLAST analysis (32). To determine the functional effect of this cluster in G1IP, we performed site-directed substitution mutagenesis to reverse the charge of four amino acid residues: R9E, R10E, R11E, and K12E = G1IP^{4E} (Fig. 3*E*).

We then in vitro expressed/translated the human Syntaxin5 (Stx5) fused to a C-terminal opsin-tag (Stx5-op) in TNT reticulocyte lysate and added recombinant cytosolic fragments of MBP-WRBcc, GST-CAMLcyt, GST-*At*GET1cc, GST-G1IPcyt, and GST-G1IP^{4E}cyt together with pancreatic rough microsomes (RMs) to the reaction mix (here "cc" refers to the cytosolic coiled-coil domain in WRB or *At*GET1, and "cyt" refers to the cytosolic N terminus of CAML or G1IP). If the C terminus of Stx5 is exposed to the ER lumen, the opsin-tag becomes glycosylated, confirming successful membrane insertion. This assay had been used previously to demonstrate that the cytosolic coiled-coil domain of WRB and the cytosolic N terminus of CAML are capable of interfering with TA protein insertion (15, 33). The ratio of glycosylated and nonglycosylated Stx5-op, determined via the band shift in immunoblot analyses, revealed that the native cytosolic domain of G1IP, but not the reverse-charged mutant version (G1IP^{4E}cyt), prevents insertion of the in vitro translated TA protein Stx5 into ER-derived microsomes (Fig. 3 *F* and *G*). The interference of the native G1IP N terminus with the mammalian machinery for TA protein insertion suggests a conserved role for this domain in binding of TRC40/GET3. However, the coiled-coil motif of *At*GET1 does not inhibit membrane insertion, indicating that the binding sites or functional residues may have diverged from those of its ortholog in mammals. These functional differences are also evident from the yeast complementation assays (Fig. 2 *C* and *D*) and underpin the

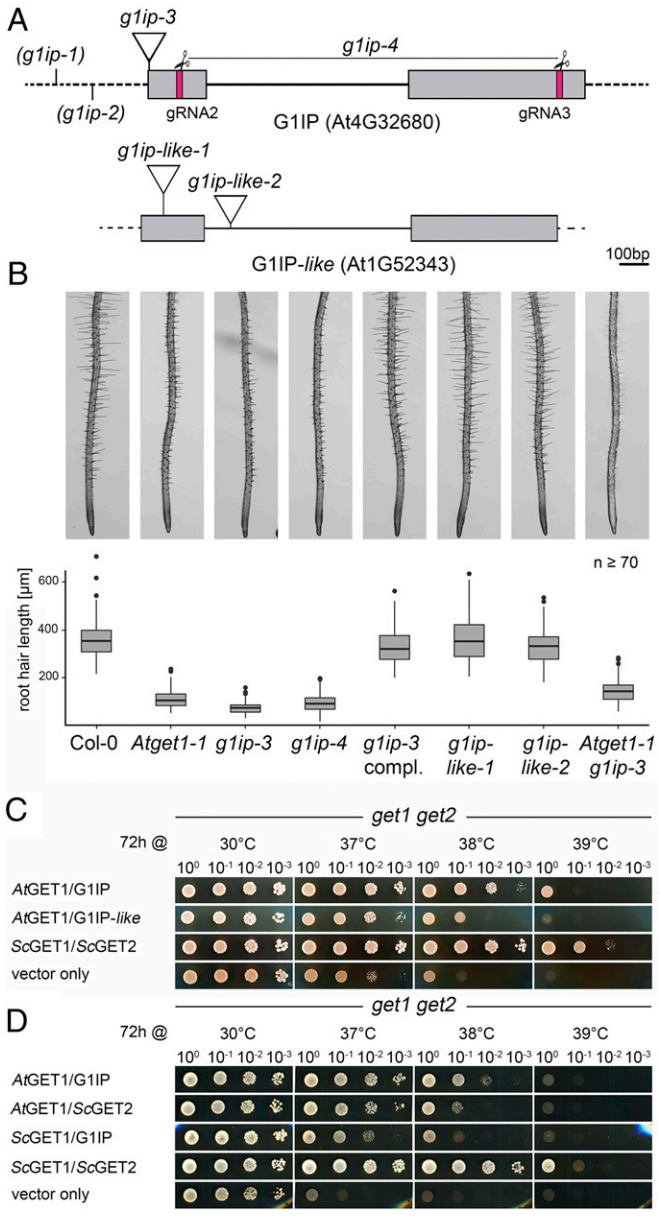

Fig. 2. G1IP phenocopies GET pathway mutants in *Arabidopsis* and partially complements a yeast GET receptor mutant in combination with *At*GET1. (*A*) Schematic illustration of the G1IP gene structure. The T-DNA in *g1ip-3* is inserted 5 bp downstream of the ATG with an additional insertion of AGTT. In *g1ip-1* and *g1ip-2*, the T-DNA insertion is within the 5′ UTR (dotted line), 333 bp and 201 bp upstream of the ATG, respectively. The *g1ip-4* line lacks the part between the CRISPR target sites indicated in red and symbolized by the scissors above. (*B*) Representative images of roots of 10-d-old mutant seedlings or complemented lines. Boxplots show quantification of root hair length of the 10 longest root hairs from at least seven seedlings per genotype. Center lines of boxes represent the median, with outer limits at the 25th and 75th percentiles. Tukey whiskers extend to 1.5 times the IQR. Outliers are depicted as black dots. (*C* and *D*) Yeast complementation analyses of the yeast *Δget1get2* double-deletion strain with different combinations of *A. thaliana* and *S. cerevisiae* proteins. Growth was monitored after 3 d in different temperatures. Genomic fragments of yeast GET1 and GET2 were used as positive controls, and empty vectors were used as negative controls. Since the T-DNA insertion in *g1ip-3* is located close to the ATG, and to confirm that the observed phenotype is a result of the insertion mutation in *G1IP*, we also performed CRISPR/Cas9 genome editing to generate a *g1ip* complete deletion mutant (*g1ip*-4). Root hair growth in this line was reduced, phenocopying the T-DNA line *g1ip-3* and thereby confirming that loss of G1IP leads to the reduced root hair growth. Simultaneous homozygous knockout of *At*GET1 and G1IP did not exacerbate the short root hair phenotype, indicating that both genes may be part of the same pathway (Fig. 2*B*). In contrast, *g1ip-like* T-DNA insertion lines exhibited WT-like root hair growth without any significant growth defects at later stages.

importance of the positively charged motif common to yeast Get2, mammalian CAML, and *Arabidopsis* G1IP. In summary, the experimental evidence presented here builds a strong case that G1IP is indeed *At*GET2, the *Arabidopsis* ortholog of yeast Get2 and mammalian CAML.

The GET Receptor Complex Shows Low Evolutionary Conservation. While interaction data and the root hair phenotype seem to confirm that *At*GET1 and G1IP/*At*GET2 act in the same pathway, sequence conservation of the two receptors is poor compared with opisthokont candidates (*SI Appendix*, Fig. S1*A*). Similarly, sequence conservation between fungal Get2 and mammalian CAML is equally poor, leading the authors who identified the connection to postulate that "mammalian cells have no genes homologous to Get2" (15).

Our finding of G1IP/*At*GET2, however, gave us an amino acid sequence with which we were able to identify numerous archaeplastidic homologs to compare with both fungal GET2 and metazoan CAML sequences (Fig. 4 and *SI Appendix*, Fig. S5). The structural similarities of the cross-kingdom proteins are striking regarding the putative number of TMDs (three), the topology of the proteins (cytosolic N terminus, luminal C terminus), and, most importantly, the positively charged N terminus (at least four arginine or lysine residues in a row; see motifs in Fig. 4). A recently published independent analysis using PSI-BLAST showed that the N-terminal Get3 interaction motif and the C-terminal membrane anchoring domain coevolve and allow the identification of candidate GET2 homologs from distantly related groups, including plants (32).

Our phylogenetic analysis of (putative) GET2 homologs from different eukaryotic groups clearly separates homologs from high-level groups (animals, fungi, and plants) (Fig. 4). Somewhat surprisingly, the Brassicales GET2 homologs are clustered separately at the bases of the eudicots. The G1IP-*like* proteins—which we now term GET2-*like*—are only found in the Rosids, clustering as a separate branch. The most striking difference within the N-terminal Get3 interaction motif is a conserved alanine residue in *At*GET2 and GET2 orthologs (*SI Appendix*, Fig. S6). *At*GET2-*like* instead features an additional glutamic acid residue, with the exception of the GET2-*like* protein from *Vitis vinifera*, which clusters at the base of the GET2-*like* proteins. The positions of the Brassicales GET2 and the GET2-*like* proteins might be explained by two whole-genome duplication events in the core Brassicales and the rosid lineages, respectively (34). These events might have led to differential loss of one copy in the Brassicales and evolution of GET2 in the rosids, although other possible explanations involving gene duplications and losses cannot be excluded.

Taken together, the structural similarities of *At*GET2 with either fungal GET2 or metazoan CAML, the network of physical interactions with other components of the *Arabidopsis* GET pathway, complementation of yeast knockouts, and the phenocopying of the loss-of-function *Arabidopsis* mutants strongly suggest that we have indeed identified the functional ortholog of GET2 in *Arabidopsis*. This discovery is consistent with a recent independent bioinformatic analysis (32) presenting candidate Get2/CAML homologs based on PSI-BLAST and allows recognition of GET2/CAML orthologs in other higher plant species or even basal Archaeplastida (*SI Appendix*, Table S1). In addition, we have identified a rosid lineage-specific homolog GET2-*like* that seems nonfunctional in the context of a plant GET pathway. This identification of the missing GET receptor in plants paves

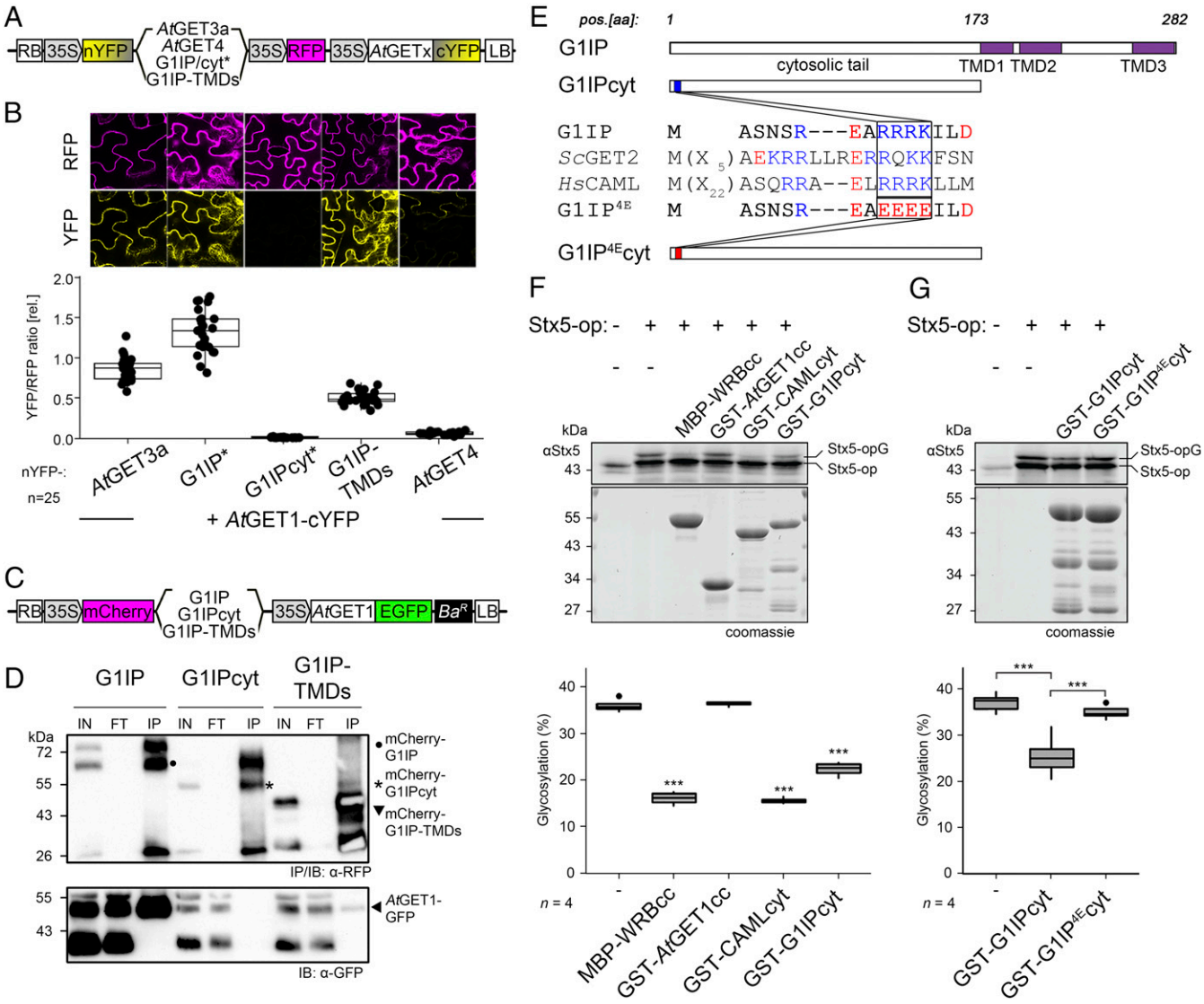

Fig. 3. The TMD region of G1IP mediates interaction with *At*GET1, and its cytosolic N terminus can interfere with the mammalian insertion system. (*A*) Schematic of the 2in1 rBiFC constructs used in *B*. G1IP and G1IPcyt were tagged C-terminally to avoid masking the N-terminal motif, marked with an asterisk. (*B*) rBiFC analysis using full-length and truncated versions of G1IP to test for interaction with *At*GET1. Exemplary CLSM images of transiently transfected *N. benthamiana* leaves are depicted. Mean fluorescence of at least 25 areas was measured in YFP and RFP channels, ratioed, and plotted to show YFP complementation. Center lines of boxes represent the median, with outer limits at the 25th and 75th percentiles. Tukey whiskers extend to 1.5 times the IQR. All values are depicted as black dots. (*C*) Schematic of the 2in1 FRET constructs used for co-IP in *D*. (*D*) Co-IP of full-length and truncated G1IP with *At*GET1, transiently expressed in *N. benthamiana* leaves. Protein extracts were immunoprecipitated with anti-RFP beads, and protein–protein interaction was detected by immunoblotting using anti-RFP and anti-GFP antibodies. IN, input; FT, flow-through; IP, immunoprecipitate. (*E*) Schematic representation of full-length, truncated, and mutated G1IP. The small alignment highlights a conserved cluster of positively charged amino acids and its charge-reversal mutation in the G1IP^{4E}cyt mutant, respectively. (*F* and *G*) Insertion assays into microsomal membranes. Stx5-op was translated in vitro in rabbit reticulocyte lysate and incubated with recombinant cytosolic fragments and pancreatic rough microsomes. Protein extracts were immunoblotted with anti-Stx5 antibody, and ER insertion was monitored via band shift reporting glycosylation. Boxplots show quantification of the immunoblots from four independent experiments. The center lines of boxes represent the median, with outer limits at the 25th and 75th percentiles. Tukey whiskers extend to 1.5 times the IQR. Outliers are depicted as black dots. ***$P < 0.001$, Student's *t* test.

the way for future research into pathway function and conservation in the eukaryotic domain of life. The absence of a more severe growth defect in GET pathway mutants of *Arabidopsis* remains puzzling and suggests the presence of additional membrane-targeting pathways and/or alternative functions of GET in plants.

Materials and Methods

Construct Generation and Plant Transformation. Most constructs were designed using Gateway technology or the Gateway-compatible cloning system 2in1 (25, 28, 35). For generation of the reverse-charged mutation of G1IP, three arginine and one lysine residue at positions 9 to 12 were exchanged with glutamic acid residues by site-directed mutagenesis as described previously (36).

PVAMP721>>GFP-myc-gG1IP was generated by classical cloning. The genomic fragment of G1IP from start codon to 261 bp downstream of the stop codon was PCR-amplified and inserted into the binary vector PVAMP721>>GFP-myc 3′ of myc.

Constructs were transformed into *Agrobacterium tumefaciens* GV3101 and used to transform Col-0 or respective mutant plants or infiltrated into *N. benthamiana* leaves (28). For the CRISPR construct, annealed oligos (forward: 5′-ATTG + protospacer; reverse: 5′-AAAC + rev-com protospacer) were

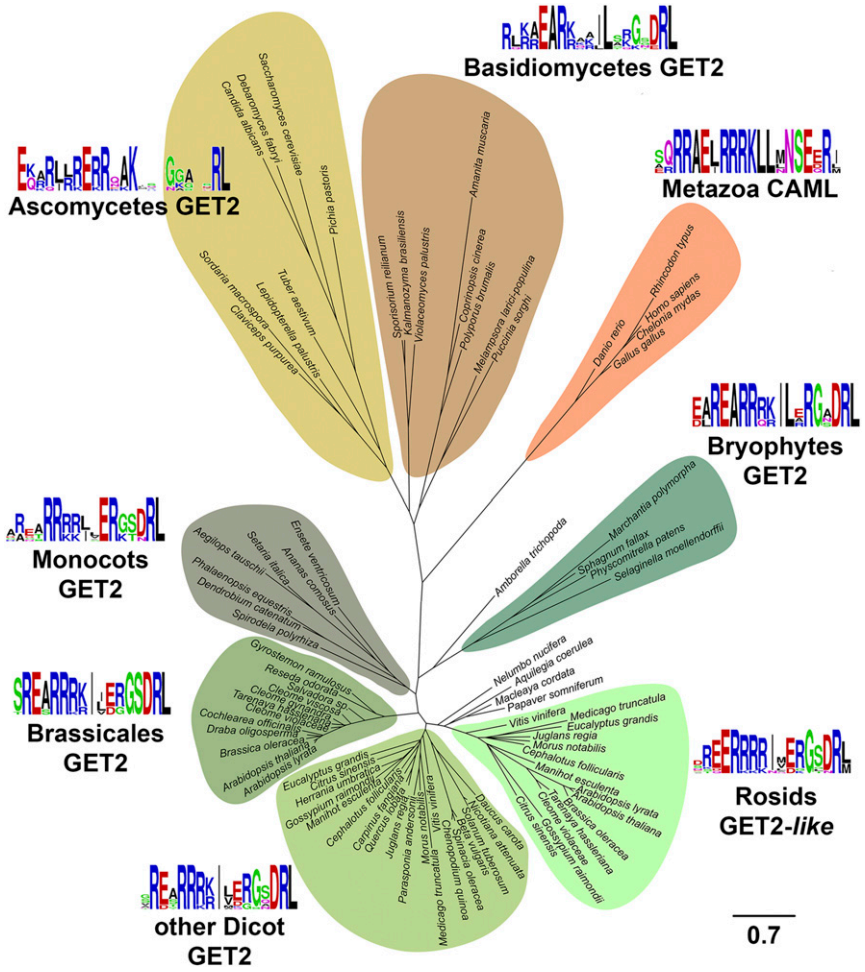

Fig. 4. Phylogenetic tree of GET2, CAML, and plant-specific GET2/GET2-like homologous proteins. A multiple alignment was generated with Muscle, and the phylogenetic tree was generated with MrBayes. The scale bar indicates expected substitutions per site. Bayesian probabilities of the branching pattern as well as accession numbers of the sequences used are provided in the corresponding cladogram in *SI Appendix*, Fig. S5.

sequentially ligated into pEn-2xChimera (37) via BbsI and Esp3I, respectively, followed by Gateway cloning into pEC-CAS9. Target sites (3′-AAGAAGTAG AATCGGAAGG-5′ and 5′-GATGATGGTGAAGAAGATAA-3′) were selected using CRISPR-P 2.0 (38). Constructs were transformed into Col-0 through floral dipping, and T1 plants were selected by red fluorescence.

Cloning of pEC-CAS9. A modified version of pDe-CAS9 (39) containing pOLE-OLE-tagRFP was digested using EcoRI. The EC promoter (40) and Cas9-attR1 fragment (39) were PCR-amplified separately with overlapping ends and combined with the vector backbone by In-Fusion cloning. The resulting vector, pEC-CAS9, was verified by restriction digest and sequencing.

Plant Material and Growth Conditions. All mutant and transgenic lines used in this work were in the Columbia (Col-0) background. T-DNA insertion lines were obtained from the Nottingham *Arabidopsis* Stock Centre (arabidopsis.info/), and insertion sites were verified by sequencing: Atget1-1 (SAIL_1210_E07) (22), Atget1-2 (GK_264D06), g1ip-1 (SALK_100089), g1ip-2 (SALK_119358), g1ip-3 (SALK_034959), g1ip-like-1 (SAIL_760_H02), and g1ip-like-2 (SALK_045533).

The CRISPR-based mutant line was generated with a dual sgRNA approach and screened using a visual selection marker (FAST-Red). Expression of Cas9 was driven by the egg cell-specific promoter EC1. Large-fragment deletion mutants were identified by PCR-based genotyping and verified by sequencing. The primer sets used for genotyping are listed in *SI Appendix*, Table S2.

Plants were grown at 22 °C under long-day conditions (16-h light/8-h dark) in soil or on half-strength Murashige and Skoog agar plates (1%; pH 5.7). Seeds were surface-sterilized with chlorine gas and stratified at 4 °C for 2 to 3 d in darkness to equalize germination.

rBiFC. Coding sequences were cloned into binary 2in1 rBiFC vectors (25) and transformed into *N. benthamiana* through syringe-mediated infiltration as described previously (28). Fluorescence intensities were measured at 3 d postinfiltration using a Leica SP8 confocal laser scanning microscope (YFP at 514 nm excitation (ex) and 520–560 nm emission (em); RFP at 561 nm ex and 565–620 nm em). YFP/RFP ratios were calculated from at least 21 different leaf regions and plotted using BoxPlotR (shiny.chemgrid.org/boxplotr/).

Subcellular Localization Analysis. Coding sequences were cloned into the Gateway vector pH7WGF2 (41) and cotransformed with an ER membrane marker (CD3-959 or CD3-960) into Col-0 through floral dipping. T1 plants were selected on hygromycin and leaves were imaged using a Leica SP8 confocal laser scanning microscope (GFP at 488 nm ex and 490–520 nm em; RFP at 561 nm ex and 565–620 nm em).

Root Hair Imaging and Measurements. Roots from 10-d-old seedlings grown on half-strength Murashige and Skoog agar plates were imaged with a Zeiss Axio Zoom V16 light microscope, and the length of the 10 longest root hairs from at least seven seedlings per genotype were measured using ImageJ ($n \geq 70$).

qPCR and RT-PCR Analysis. Total RNA was isolated from various plant tissues (100 mg) using the GeneMATRIX Universal RNA Purification Kit (Roboklon). Then 1 μg of each sample was converted into cDNA using the Protoscript II-First-Strand cDNA Synthesis Kit (New England BioLabs). cDNA was diluted 1:5 and quantified on the CFX96 Real-Time PCR System (Bio-Rad) using GoTag qPCR Master Mix (Promega) with SYBR Green. Transcript levels were calculated by the 2-ΔCt method and normalized to ACT2 expression. For

semiquantitative RT-PCR, first-strand cDNA was amplified for 30 cycles and verified by agarose gel electrophoresis. Primer sets used for qPCR and RT-PCR are listed in *SI Appendix*, Table S2.

Yeast Complementation Assay. *Saccharomyces cerevisiae* genes with part of the 5′ and 3′ flanking regions (~0.5 kb) were cloned into low-copy number ARS/CEN vectors. *A. thaliana* genes (full-length CDS) were constitutively expressed from 2μ origin plasmids using the yeast PMA1 promoter. The *Δget1get2* double-deletion mutant (MATa his3Δ1 leu2Δ0 met15Δ0 ura3Δ0 ygl020c::KanR yer083c::NatR) (19) was cotransformed as described previously (42) and dropped in 10-fold serial dilutions in vector-selective medium (complete supplement medium [CSM] L-, U-) and grown at different temperatures for 3 d.

Creation of 2in1 Co-IP Vectors (mVenus/3xHA). The new set of Gateway-compatible 2in1 co-IP vectors (pCoIP-2in1-NN, -NC, -CN, -CC) was generated by classical cloning. RPS5a driven N- and C-terminally 3xHA-tagged R3R2 expression cassettes were generated by replacing the 35S promoter in pUC57-Tec-*N*-HA and pUC35S-R3R2-3xHA (NarI/HpaI) with the RPS5a promoter (1,684 bp), which was PCR-amplified and flanked by NarI-StuI/NaeI (blunt end, like HpaI) restriction sites (pUC-RPS-HA-lacZ and pUC-RPS-lacZ-HA). The resulting expression cassettes were excised via StuI and inserted into pBBb (35) via EcoICRI (blunt end, like StuI) to yield the intermediate vectors pCoIP-intA and pCoIP-intB. Another pUC helper vector, pUC-RPS5a::R1R4, was created by introducing the RPS5a promoter via NarI/NaeI into pUC57-Tec-*N*-myc. mVenus was PCR- amplified (NaeI/SpeI) and inserted via NaeI/HpaI 5′ of the R1R4 expression cassette (pUC-RPS5-Ven-R1R4). To introduce mVenus at the C terminus, PCR-amplified mVenus-TGA (NaeI/PsiI) was inserted into pUC-RPS5a::R1R4 via PsiI (pUC-RPS5-R1R4-Ven). For the final 2in1 vector assembly, the intermediate vectors pCoIP-intA and pCoIP-intB were linearized via AfeI, and the R3R2 and R1R4 expression cassettes were inserted (StuI/FspI). All vectors were verified by restriction digest and sequencing.

Co-IP Analysis: Stable Gene Expression in *Arabidopsis*. Here 3 g of *Arabidopsis* seedlings were harvested after 10 d under continuous light. Cells were lysed by mortar grinding in liquid nitrogen and thawed in lysis buffer (50 mM Tris pH 7.5, 150 mM NaCl, 1% Triton X-100; 1.43 mL/g) supplemented with protease inhibitor mixture (cOmplete EDTA-free; Roche). Cell debris was removed by centrifugation and filtration through two layers of Miracloth. Then 2.5 mL of supernatant was mixed with 2 mL of lysis buffer and incubated with anti-GFP beads (25 μL, GFP-trap; Chromotek) for 2 h at 4 °C under mild rotation. Beads were collected by centrifugation, transferred onto spin columns, and washed six times with washing buffer (50 mM Tris pH 7.5, 150 mM NaCl, and 0.5% Triton X-100) supplemented with protease inhibitor mixture. (Co-) Immunoprecipitated proteins were eluted with 2× Laemmli buffer (+ 3% β-mercaptoethanol) at 80 °C for 5 min, separated by sodium dodecyl sulfate polyacrylamide gel electrophoresis (SDS-PAGE), and detected by Western blot analysis (anti-HA peroxidase from rat IgG1 [Roche, 1:1,000], anti-GFP from mouse IgG1κ [Roche, 1:1,000], and anti-mouse IgG [Fc-specific] produced in goat [Sigma-Aldrich, 1:10,000]).

Co-IP Analysis: Transient Gene Expression in *N. Benthamiana*. FRET 2in1 destination vectors containing monomeric enhanced green fluorescent protein (mEGFP) and mCherry (pFRETgc-2in1) were used to transiently express recombinant proteins in *N. benthamiana* for co-IP analysis (28, 35). Leaf material (150 to 600 mg) was harvested at 3 d postinfiltration and homogenized after freezing in liquid nitrogen. Lysis buffer (25 mM Tris pH 8.0, 150 mM NaCl, 1% Nonidet P-40, and 0.5% Na-deoxycholate) supplemented with protease inhibitor mixture and 2 mM DTT was added and incubated for 1 h at 4 °C with mild rotation. After centrifugation, the supernatant was mixed with 20 to 25 μL of RFP beads (RFP-trap; Chromotek) and then incubated for 1 h at 4 °C with mild rotation. Beads were collected by centrifugation, transferred onto spin columns, and rinsed twice with lysis buffer, followed by six washes with wash buffer (25 mM Tris pH 8.0 and 150 mM NaCl). (Co-) Immunoprecipitated proteins were eluted with 2× Laemmli buffer (+ 3.5% β-mercaptoethanol) and then heated at 65 °C for 15 min (membrane proteins) or at 95 °C for 5 min (soluble proteins). Proteins were separated by SDS-PAGE and detected by Western blot analysis (anti-RFP from mouse [Chromotek, 1:2,500], anti-GFP from mouse IgG1κ [Roche, 1:1,000], and anti-mouse IgG [Fc-specific] produced in goat [Sigma-Aldrich, 1:10,000]).

Protein Purification. *Escherichia coli* BL21 DE3 cells were transformed with GST-tagged versions of the cytosolic portions of *At*GET1 and G1IP. Expression was induced with 200 μM isopropyl β-d-1-thiogalactopyranoside in 1 L of 2YT-3% glycerol cultures at an OD_{600} of 0.5. The cell pellet was collected after 3 h at 30 °C and lysed by sonification in ice-cold purification buffer (20 mM Hepes, 2% glycerol, 150 mM potassium acetate, 5 mM magnesium acetate, 1 mM EDTA, 1 mM DTT, and 1 mM PMSF, pH 7.4). The lysate was cleared by centrifugation at 100.000 × *g* for 30 min and then incubated with glutathione Sepharose resin (GE Healthcare). After 1 h of binding, the resin was washed sequentially with purification buffer, purification buffer containing 5 mM ATP, and purification buffer for 10 min. GST-tagged protein was eluted with purification buffer containing 20 mM glutathione.

Expression of the N-terminal domain of CAML (GST-CAMLcyt) and the WRB coiled-coil domain (MBP-WRBcc) was carried out as described previously (15, 33).

Stx5-op In Vitro Transcription/Translation and Insertion Assay into Microsomes. Reactions were performed in the TnT Quick Coupled Transcription/Translation System (Promega) as described previously (17, 43) with some modifications. Stx5-op synthesis was induced with 100 ng of pGem3z-Stx5-op in 4.5 μL of TNT reticulocyte lysate for 90 min at 30 °C. Where indicated, equimolar amounts (5 μM) of recombinant cytosolic fragments (MBP-WRBcc, GST-CAMLcyt, GST-*At*GET1, GST-G1Ipcyt, and GST-G1IP4Ecyt) and pancreatic RMs were added to the reaction mix after Stx5 translation was completed. After 90 min of incubation at 30 °C with the RMs, the reaction was stopped with SDS loading buffer, followed by analysis by Western blot with rabbit anti-Stx5 antibody (Synaptic Systems; 110053).

Multiple Alignments and Construction of Phylogenetic Trees. Multiple alignments were generated with Muscle in MEGA6.06 (44, 45). Phylogenetic analyses were performed with MrBayes 3.2.7a, with 500,000 generations (46).

Data Availability. All study data are included in the main text and *SI Appendix*.

ACKNOWLEDGMENTS. We thank Simon Klesen for cloning and providing the pEC-CAS9 vector and Eva Schwörzer and Laure Grefen for excellent technical assistance. The IP-MS analysis was performed at the Proteomics facility of the University of Tübingen; we are grateful to Mirita Franz for helpful advice during data analyses. This project was supported through a Carl Zeiss doctoral fellowship to D.G.M. and funding from the German Research Foundation to M.N. (NO 407/7-1), B.S. (SFB1190-P04), M.B. (SFB1101-B01) and C.G. (Emmy Noether fellowship GR 4251/1-1, GR 4251/1-2, and SFB1101-A06).

1. S. Shao, R. S. Hegde, Membrane protein insertion at the endoplasmic reticulum. *Annu. Rev. Cell Dev. Biol.* **27**, 25–56 (2011).
2. V. Lipka, C. Kwon, R. Panstruga, SNARE-ware: The role of SNARE-domain proteins in plant biology. *Annu. Rev. Cell Dev. Biol.* **23**, 147–174 (2007).
3. G. Jürgens *et al*., Plant cytokinesis: A tale of membrane traffic and fusion. *Biochem. Soc. Trans.* **43**, 73–78 (2015).
4. R. Jahn, R. H. Scheller, SNAREs—Engines for membrane fusion. *Nat. Rev. Mol. Cell Biol.* **7**, 631–643 (2006).
5. U. S. Chio, H. Cho, S. O. Shan, Mechanisms of tail-anchored membrane protein targeting and insertion. *Annu. Rev. Cell Dev. Biol.* **33**, 417–438 (2017).
6. J. W. Chartron, C. J. Suloway, M. Zaslaver, W. M. Clemons Jr, Structural characterization of the Get4/Get5 complex and its interaction with Get3. *Proc. Natl. Acad. Sci. U.S.A.* **107**, 12127–12132 (2010).
7. Y. W. Chang *et al*., Crystal structure of Get4-Get5 complex and its interactions with Sgt2, Get3, and Ydj1. *J. Biol. Chem.* **285**, 9962–9970 (2010).
8. G. Bozkurt *et al*., Structural insights into tail-anchored protein binding and membrane insertion by Get3. *Proc. Natl. Acad. Sci. U.S.A.* **106**, 21131–21136 (2009).
9. A. Mateja *et al*., The structural basis of tail-anchored membrane protein recognition by Get3. *Nature* **461**, 361–366 (2009).
10. M. E. Rome, M. Rao, W. M. Clemons, S. O. Shan, Precise timing of ATPase activation drives targeting of tail-anchored proteins. *Proc. Natl. Acad. Sci. U.S.A.* **110**, 7666–7671 (2013).
11. H. B. Gristick *et al*., Crystal structure of ATP-bound Get3-Get4-Get5 complex reveals regulation of Get3 by Get4. *Nat. Struct. Mol. Biol.* **21**, 437–442 (2014).
12. K. Kubota, A. Yamagata, Y. Sato, S. Goto-Ito, S. Fukai, Get1 stabilizes an open dimer conformation of get3 ATPase by binding two distinct interfaces. *J. Mol. Biol.* **422**, 366–375 (2012).
13. F. Wang, C. Chan, N. R. Weir, V. Denic, The Get1/2 transmembrane complex is an endoplasmic-reticulum membrane protein insertase. *Nature* **512**, 441–444 (2014).
14. S. Stefer *et al*., Structural basis for tail-anchored membrane protein biogenesis by the Get3-receptor complex. *Science* **333**, 758–762 (2011).
15. Y. Yamamoto, T. Sakisaka, Molecular machinery for insertion of tail-anchored membrane proteins into the endoplasmic reticulum membrane in mammalian cells. *Mol. Cell* **48**, 387–397 (2012).

16. S. F. Colombo *et al*., Tail-anchored protein insertion in mammals: Function and reciprocal interactions OF the two subunits of the TRC40 receptor. *J. Biol. Chem.* **291**, 15292–15306 (2016).
17. J. Rivera-Monroy *et al*., Mice lacking WRB reveal differential biogenesis requirements of tail-anchored proteins in vivo. *Sci. Rep.* **6**, 39464 (2016).
18. H. J. F. Carvalho, A. Del Bondio, F. Maltecca, S. F. Colombo, N. Borgese, The WRB subunit of the Get3 receptor is required for the correct integration of its partner CAML into the ER. *Sci. Rep.* **9**, 11887 (2019).
19. M. Schuldiner *et al*., The GET complex mediates insertion of tail-anchored proteins into the ER membrane. *Cell* **134**, 634–645 (2008).
20. S. Stefanovic, R. S. Hegde, Identification of a targeting factor for posttranslational membrane protein insertion into the ER. *Cell* **128**, 1147–1159 (2007).
21. R. Srivastava, B. E. Zalisko, R. J. Keenan, S. H. Howell, The GET system inserts the tail-anchored protein, SYP72, into endoplasmic reticulum membranes. *Plant Physiol.* **173**, 1137–1145 (2017).
22. S. Xing *et al*., Loss of GET pathway orthologs in Arabidopsis thaliana causes root hair growth defects and affects SNARE abundance. *Proc. Natl. Acad. Sci. U.S.A.* **114**, E1544–E1553 (2017).
23. K. L. Auld *et al*., The conserved ATPase Get3/Arr4 modulates the activity of membrane-associated proteins in Saccharomyces cerevisiae. *Genetics* **174**, 215–227 (2006).
24. U. Omasits, C. H. Ahrens, S. Müller, B. Wollscheid, Protter: Interactive protein feature visualization and integration with experimental proteomic data. *Bioinformatics* **30**, 884–886 (2014).
25. C. Grefen, M. R. Blatt, A 2in1 cloning system enables ratiometric bimolecular fluorescence complementation (rBiFC). *Biotechniques* **53**, 311–314 (2012).
26. J. Mergner *et al*., Mass-spectrometry-based draft of the Arabidopsis proteome. *Nature* **579**, 409–414 (2020).
27. S. Xing, N. Wallmeroth, K. W. Berendzen, C. Grefen, Techniques for the analysis of protein-protein interactions in vivo. *Plant Physiol.* **171**, 727–758 (2016).
28. D. G. Mehlhorn, N. Wallmeroth, K. W. Berendzen, C. Grefen, 2in1 vectors improve in planta BiFC and FRET analyses. *Methods Mol. Biol.* **1691**, 139–158 (2018).
29. Y. W. Chang *et al*., Interaction surface and topology of Get3-Get4-Get5 protein complex, involved in targeting tail-anchored proteins to endoplasmic reticulum. *J. Biol. Chem.* **287**, 4783–4789 (2012).
30. F. Vilardi, M. Stephan, A. Clancy, A. Janshoff, B. Schwappach, WRB and CAML are necessary and sufficient to mediate tail-anchored protein targeting to the ER membrane. *PLoS One* **9**, e85033 (2014).
31. K. Powis *et al*., Get3 is a holdase chaperone and moves to deposition sites for aggregated proteins when membrane targeting is blocked. *J. Cell Sci.* **126**, 473–483 (2013).
32. N. Borgese, Searching for remote homologs of CAML among eukaryotes. *Traffic* **21**, 647–658 (2020).
33. F. Vilardi, H. Lorenz, B. Dobberstein, WRB is the receptor for TRC40/Asna1-mediated insertion of tail-anchored proteins into the ER membrane. *J. Cell Sci.* **124**, 1301–1307 (2011).
34. M. S. Barker, H. Vogel, M. E. Schranz, Paleopolyploidy in the Brassicales: Analyses of the Cleome transcriptome elucidate the history of genome duplications in Arabidopsis and other Brassicales. *Genome Biol. Evol.* **1**, 391–399 (2009).
35. A. Hecker *et al*., Binary 2in1 vectors improve in planta (co-) localisation and dynamic protein interaction studies. *Plant Physiol.* **168**, 776–787 (2015).
36. A. Karnik, R. Karnik, C. Grefen, SDM-Assist software to design site-directed mutagenesis primers introducing "silent" restriction sites. *BMC Bioinformatics* **14**, 105 (2013).
37. J. Durr, R. Papareddy, K. Nakajima, J. Gutierrez-Marcos, Highly efficient heritable targeted deletions of gene clusters and non-coding regulatory regions in Arabidopsis using CRISPR/Cas9. *Sci. Rep.* **8**, 4443 (2018).
38. H. Liu *et al*., CRISPR-P 2.0: An improved CRISPR-Cas9 tool for genome editing in plants. *Mol. Plant* **10**, 530–532 (2017).
39. F. Fauser, S. Schiml, H. Puchta, Both CRISPR/Cas-based nucleases and nickases can be used efficiently for genome engineering in Arabidopsis thaliana. *Plant J. Cell Mol. Biol.* **79**, 348–359 (2014).
40. Z. P. Wang *et al*., Egg cell-specific promoter-controlled CRISPR/Cas9 efficiently generates homozygous mutants for multiple target genes in Arabidopsis in a single generation. *Genome Biol.* **16**, 144 (2015).
41. M. Karimi, A. Depicker, P. Hilson, Recombinational cloning with plant gateway vectors. *Plant Physiol.* **145**, 1144–1154 (2007).
42. L. Y. Asseck, N. Wallmeroth, C. Grefen, ER membrane protein interactions using the split-ubiquitin system (SUS). *Methods Mol. Biol.* **1691**, 191–203 (2018).
43. J. Pfaff *et al*., Emery-Dreifuss muscular dystrophy mutations impair TRC40-mediated targeting of emerin to the inner nuclear membrane. *J. Cell Sci.* **129**, 502–516 (2016).
44. K. Tamura, G. Stecher, D. Peterson, A. Filipski, S. Kumar, MEGA6: Molecular evolutionary genetics analysis version 6.0. *Mol. Biol. Evol.* **30**, 2725–2729 (2013).
45. R. C. Edgar, MUSCLE: Multiple sequence alignment with high accuracy and high throughput. *Nucleic Acids Res.* **32**, 1792–1797 (2004).
46. F. Ronquist, J. P. Huelsenbeck, MrBayes 3: Bayesian phylogenetic inference under mixed models. *Bioinformatics* **19**, 1572–1574 (2003).